

Chiral tunneling of topological states for giant longitudinal spin Hall angle

K. M. Masum Habib,* Redwan N. Sajjad, and Avik W. Ghosh
*Department of Electrical and Computer Engineering
 University of Virginia, Charlottesville, VA 22904*

We show that the chiral tunneling of helical surface states in a 3D Topological Insulator pn junction (TIPNJ) allows only the Klein tunneling modes to pass through. This leads to real-spin filtering in TIPNJ which is analogous to the pseudo-spin filtering in graphene. All other modes are reflected back from the junction while their spins are flipped due to spin-momentum locking. Consequently, the spin current increases while the dissipative charge current decreases, leading to an extremely high ‘longitudinal’ spin Hall angle (up to 20) at the reflected end and high spin polarization at the transmitted end. Our numerical results verified the robustness of our analytical prediction for gate tunable spin current and large longitudinal spin Hall angle in presence of edge reflections at room temperature.

Since their theoretical prediction and experimental verification in quantum wells[1] and bulk crystals[2], Topological insulators (TI) have been of great interest in condensed matter physics, even prompting their classification as a new state of matter[3]. The large spin orbit coupling in a TI leads to an inverted band (s like valence band, p like conduction band) separated by a bulk bandgap. Symmetry considerations dictate that setting such a TI against a normal insulator (including vacuum) forces a band crossing at their interface, leading to gapless edge (for 2D) and surface (for 3D) states protected by time reversal symmetry. The spin-momentum locking of TI surface states has strong implications for Spin Hall effect. The discovery of Giant Spin Hall Effect (GSHE)[4] shows a possible way for efficient generation of spin current using its internal gain. The gain is parameterized by the spin Hall angle $\theta_H = \frac{2I_s/\hbar}{I_q/q}$ where I_s and I_q are the spin and charge currents respectively. θ_H for various metals and metal alloys has been found to vary between 0.07-0.3[4–6]. Recently, Bi_2Se_3 based TI has been reported to have $\theta_H = 2 - 3.5$ [7] and has been shown to switch a soft ferromagnet at low temperature[8].

In recent years, the transport physics of graphene based pn junction has been studied both theoretically[9–11] and experimentally[12] because of its unique tunneling characteristics. The tunneling across the junction demonstrates an angle dependent transmission probability[9] originating from the chiral nature of graphene electrons. With a split pn junctions, it has been shown that the junction acts as a filter for pseudospins and only allows very low angle electrons to pass through[9]. The resemblance of low energy Hamiltonian of TI $\hat{H} = v_F \hat{z} \cdot (\boldsymbol{\sigma} \times \mathbf{p})$ [3] with that of graphene $H = v_F \boldsymbol{\sigma} \cdot \mathbf{p}$ suggests that the chiral tunneling in combination with spin-momentum locking in TI pn junctions[13–15] might have implications for spintronics.

In this letter, we show that chiral tunneling in a split gate TIPNJ (Fig. 1) only allows electrons with very small incident angle to pass through and all other electrons are reflected back to the source in the same way as graphene.

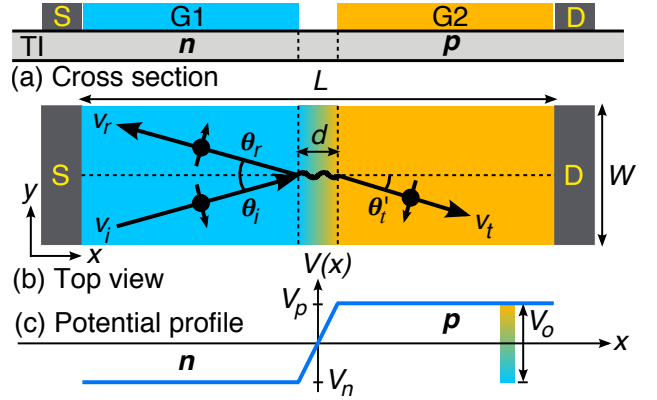


FIG. 1. (a) Cross section of the TIPNJ. The source, the drain and the gates are placed on the top surface of the 3D TI. The spatially separated gates create a graded pn junction. (b) Top view of the device showing the directions of incident, reflected and transmitted electrons and their spins. The spin of the reflected wave is flipped due to spin-momentum locking which enhances the spin current at source. (c) Linear approximation of potential energy profile.

As a result, charge current going through the junction decreases. Due to spin-momentum locking, the injected electrons have down spin but the reflected electrons have up spin which enhances the spin current at the source contact. These result in an extraordinarily large ‘longitudinal’ spin Hall angle. The term longitudinal refers to the fact that flow of spin and charge are along the same direction in TIPNJ unlike transverse direction in GSHE and in TI with a step potential[16]. We show below that in a split-gate, symmetrically doped TIPNJ, the longitudinal spin Hall angle at the source contact is,

$$\theta_H \approx \frac{1 + R_{av}}{1 - R_{av}} \approx 2\sqrt{\frac{qV_0 d}{\hbar v_F}} - 1 \quad (1)$$

for small bias. Here, R_{av} is the reflection probability averaged over all modes, V_0 is the built in potential of the TIPNJ and d is the split between the gates. For a device with $d = 100$ nm and $V_0 = 0.3$ V, θ_H at source

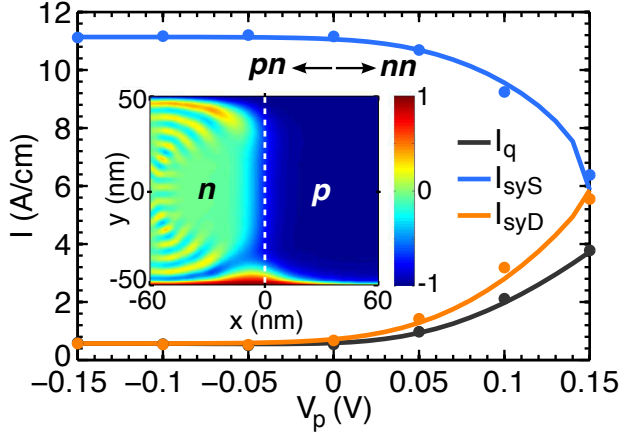


FIG. 2. Charge and spin current vs. gate voltage on the p -side (V_p) at $V_n = 0.15$ V. The charge and the spin current at drain are reduced whereas the spin current at source is enhanced as the device is driven from nn ($V_p = 0.15$ V) to pn ($V_p = -0.15$ V) regime. The analytical (solid lines) and the numerical (circles) results are in good agreement. **Inset:** Spin polarization in symmetric pn regime. In the p region only transmitted modes (spin down) exist resulting in strong polarization (blue). In the n region, both the incident (spin down) and the reflected modes (spin up) exist, hence it is mostly unpolarized (green).

is ~ 20 and at drain it is ~ 1 . We also show below that the p region is highly spin polarized since only the small angle modes (with spin- y) exist there.

The cross section and the top view of the model TIPNJ device are shown in Fig. 1a and 1b respectively. The 3D TI is assumed to be Bi_2Se_3 which has the largest bulk bandgap of 350 meV[2]. The source (S) and the drain (D) contact are placed on the top surface of the 3D TI slab. We assume that conduction of electron only takes place on the top surface of the TI which is a good approximation considering that the device is operated within the bulk bandgap to minimize the bulk conduction and only a small part of the total current goes through the bottom surface[17]. The p and n regions are electrically doped using two external gates G1 and G2 separated by the split distance d . Such gate controlled doping of 3D TI surface states has been demonstrated experimentally for Bi_2Se_3 [18]. The device has a built-in potential $V_o = V_p + V_n$ distributed between the p and n regions as shown in Fig. 1c assuming a linear potential profile inside the split region. Electrons are injected from source and collected at drain by a bias voltage V_D .

The solid lines in Fig. 2 shows the charge and spin current versus gate bias of the p region calculated using Eqs. 5-10 for a device with length $L = 120$ nm, width $W = 100$ nm, split length $d = 100$ nm, drain bias $V_D = 0.1$ V and gate voltage $V_n = 0.15$ V at room temperature. When the gate voltage of p region $V_p = 0.15$ V, the channel is a perfect nn type with uniform poten-

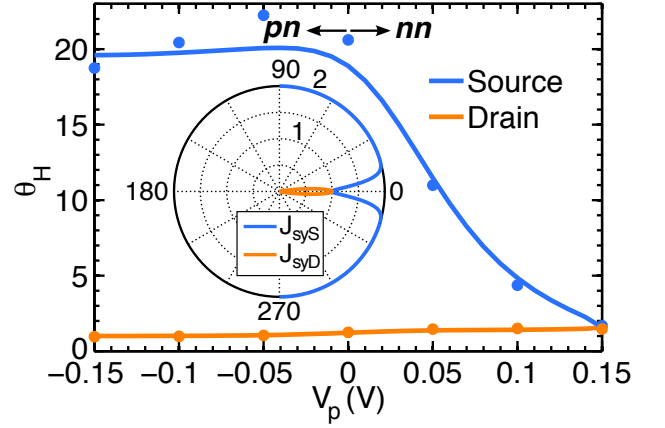


FIG. 3. Longitudinal spin Hall angle θ_H vs. V_p at $V_n = 0.15$ V. θ_H increases at source as the device is driven from nn to pn regime. The solid lines and the circles represent analytical and numerical results respectively. **Inset:** Angle dependent normalized spin current densities at source and drain in symmetric pn regime. Spin current at drain (J_{syD}) is carried by small angle modes only. All other modes contribute to source spin current (J_{syS}) twice: (1) when they are injected and (2) when they are reflected back since their spins are flipped.

tial profile. Thus, all the modes are allowed to transmit from the source to the drain and there is no reflection. Hence, the charge current is maximum, spin current at the source and drain are equal and $\theta_H = \pi/2$ as shown in Fig. 3. When the gate voltage V_p is decreased to -0.15 V, the potential profile is no longer uniform, the channel becomes a pn junction and most of the electrons are reflected back from the junction and therefore, charge current is reduced. Since the incident and reflected waves have opposite spins, the reflected waves enhances the spin current at the source end and θ_H becomes large at the source contact. In the drain contact, however, only the transmitted electrons are collected and θ_H remains close to 1. Thus, θ_H changes from 1.5 to 20 at source contact and remains close to 1 at the drain when the device is driven from the nn to the pn regime.

The discrete points in Figs. 2-3 were calculated using the non-equilibrium Green's function (NEGF) formalism and the discretized k.p Hamiltonian, which captures the effects of edge reflections. To avoid the well known Fermion doubling problem[19] on the discrete lattice, we added a σ^z term to the TI Hamiltonian, $H = v_F \hat{z} \cdot (\boldsymbol{\sigma} \times \mathbf{p}) + \sigma^z (k_x^2 + k_y^2)$ as suggested in Ref. [20]. We discretized this Hamiltonian using finite difference method to obtain real space Hamiltonian needed for the NEGF formalism. In order to calculate the charge and spin currents, we adopted the current density operator[21], $I_{op} = \frac{1}{\hbar} \{ G^n \Sigma_m^\dagger - \Sigma_m G^n + G \Sigma_m^{in} - \Sigma_m^{in} G^\dagger \}$ where G^n is the electron correlation function, Σ_m is the self-energy of contact $m \in \{S, D\}$ and Σ_m^{in} is the in scat-

tering matrix. The charge and spin currents are then given by, $I_q(E) = q\text{Tr}\{I_{op}\}$ and $I_s(E) = \frac{\hbar}{2}\text{Tr}\{\boldsymbol{\sigma}I_{op}\}$ respectively. Since equilibrium spin current exists on the TI surface[22], this spin current includes both equilibrium and non-equilibrium components. In order to obtain the non-equilibrium spin current, first we calculate equilibrium spin current, I_{s_0} by setting $\mu_S = \mu_D = -qV_D$ where, μ_S and μ_D are chemical potentials of the source and the drain contacts respectively. Then we calculate total (equilibrium + non-equilibrium) spin current I_s by setting $\mu_S = 0$ and $\mu_D = -qV_D$. Finally, the total non-equilibrium spin current is obtained using $I_{s_{neq}}(E) = I_s(E) - I_{s_0}(E)$ and integrating over all energies. The agreement between the numerical and the analytical results shown in Figs. 2 and 3 indicates that the physics described here is robust against the edge reflection and finite drain bias at room temperature.

Let us now derive Eq. 1 and analyze the underlying physics. We start with the effective Hamiltonian for 3D TI surface states and follow the similar procedure as described in Ref.[23] to obtain the continuity equation for spin, $\frac{\partial \mathbf{s}}{\partial t} = -\nabla \cdot \hat{\mathbf{J}}_s + \hat{\mathbf{J}}_\omega$. Here, $\hat{\mathbf{J}}_s$ is a rank 2 tensor describing the translational motion of spin and $\hat{\mathbf{J}}_\omega$ is a vector describing the rate of change of spin density due to spin precession at location \mathbf{r} and time t . The quantity $\hat{\mathbf{J}}_\omega$ is also referred to as spin torque[23]. Among nine elements of $\hat{\mathbf{J}}_s$, only \hat{J}_{sy}^x and \hat{J}_{sx}^y are nonzero for TI with

$$\hat{J}_{sy}^x = -\frac{\hbar v_F}{2} \mathbf{I} \quad \text{and} \quad \hat{J}_{sx}^y = -\frac{\hbar v_F}{2} \mathbf{I}. \quad (2)$$

The current density operator J_{sy}^x describes spin current carried by spin- y along \hat{x} direction etc. At steady state, $\nabla \cdot \hat{\mathbf{J}}_s = \hat{\mathbf{J}}_\omega$ and therefore, for a two terminal device shown in Fig. 1, the difference between the spin currents at the source and the drain terminal is the spin torque generated by the TIPNJ. Following the same procedure, we obtain the charge current density operators

$$\hat{J}^x = -qv_F \sigma^y \quad \text{and} \quad \hat{J}^y = qv_F \sigma^x \quad (3)$$

where \hat{J}^x describes the motion of electrons moving along the \hat{x} direction. For the two terminal device shown in Fig 1, since there is no net charge or spin transfer in \hat{y} direction, $J_{sx}^y = 0$ and $J^y = 0$.

The wavefunction of an electron incident from the source contact with an angle θ_i (see Fig. 1) and energy E can be written as a two component spinor, $|\psi_i\rangle = 1/\sqrt{2A}(1 - s_i i e^{i\theta_i})^T e^{i\mathbf{k}_i \cdot \mathbf{r}}$ where $A = WL$ is area of the device, $s_i = \text{sgn}(E + qV_n)$ and \mathbf{k}_i is the wavevector with magnitude $k_i = \frac{|E + qV_n|}{\hbar v_F}$ and angle θ_i . Similarly, the reflected and transmitted waves are $|\psi_r\rangle = 1/\sqrt{2A}(1 - s_i i e^{-i\theta_i})^T e^{i\mathbf{k}_r \cdot \mathbf{r}}$ and $|\psi_t\rangle = 1/\sqrt{2A}(1 - s_t i e^{i\theta_t})^T e^{i\mathbf{k}_t \cdot \mathbf{r}}$ respectively, where $k_r = k_i$, $s_t = \text{sgn}(E - qV_p)$ and $k_t = \frac{|E - qV_p|}{\hbar v_F}$. Since the potential variation is only along \hat{x} direction, the \hat{y} component of

wavevector must be conserved at the pn junction interface and $k_i \sin \theta_i = k_t \sin \theta_t$. This is so called Snell's law for electrons on the 3D TI surface. The conduction and the valence bands of TI surface state have opposite helicity for energies $E < qV_p$. Hence, the group velocity and the wavevector of the transmitted wave are antiparallel and $\theta_t = \pi - \theta_t'$. However, for $E > qV_p$, group velocity and wavevector are parallel. Therefore, the conservation of momentum along \hat{y} and the helicity of TI yield the relationship between the transmission angle and the incident angle as,

$$\theta_t = \begin{cases} \sin^{-1} \left[\frac{E + qV_n}{E - qV_p} \sin \theta_i \right] & \text{if } E > qV_p \\ \pi - \sin^{-1} \left[\frac{E + qV_n}{E - qV_p} \sin \theta_i \right] & \text{otherwise.} \end{cases} \quad (4)$$

When the incident angle θ_i for an electron is greater than the critical angle $\theta_c = \sin^{-1} \left[\frac{E - qV_p}{E + qV_n} \right]$, the \sin^{-1} functions in Eq. 4 become \sinh^{-1} , the transmission angle becomes a complex number and the electron is reflected back to the source.

In absence of the incoherent scattering, the energy of an electron is conserved which implies that the wavevector inside $-d/2 < x < d/2$ region must vary as a function of x in accordance with $k_t(x) = \frac{|E - V(x)|}{\hbar v_F}$. Since the y component of $\mathbf{k}_t(x)$ cannot change, the x component must be a function of x and given by $k_{tx} = \sqrt{k_t^2(x) - k_t^2 \sin^2 \theta_i}$. If the incident angle θ_i of an electron is such that $k_t(x) < k_{iy}$, it will go through an exponential decay inside the linear potential region. Therefore, the wavefunction of the transmitted wave within this energy range for $x > d/2$ is, $|\psi_t\rangle = 1/\sqrt{2A}(1 - s_t i e^{i\theta_t})^T e^{i(k_{tx}x + k_{ty}y)} e^{-\int_{-d/2}^{d/2} \kappa_{tx} I(x) dx}$ according to the WKB approximation, where k_{txr} and κ_{txI} are real and imaginary parts of k_{tx} . Since both incident and reflected waves exist inside the n region, the wavefunction for $x < -d/2$ is $|\psi\rangle = |\psi_i\rangle + r|\psi_r\rangle$ where r is the reflection coefficient. However, only transmitted wave exist inside the p region. Therefore, the wavefunction for $x > d/2$ is $|\psi\rangle = t|\psi_t\rangle$ where t is the transmission coefficient. Assuming $d = 0$ and matching the wavefunction at the interface $x = 0$, we obtain the transmission coefficient as $t = \frac{s_i e^{i\theta_i} + s_i e^{-i\theta_i}}{s_i e^{-i\theta_i} + s_t e^{i\theta_t}}$. Since the wavefunctions are exponentially decayed for graded pn junction (with $d \neq 0$), the general expression for transmission coefficient is

$$t = \frac{s_i e^{i\theta_i} + s_i e^{-i\theta_i}}{s_i e^{-i\theta_i} + s_t e^{i\theta_t}} e^{-\int_{-d/2}^{d/2} \kappa_{tx} I(x) dx} \quad (5)$$

which is valid for all energies.

Consider an electron injected from the source at angle θ_i and energy E is transmitted from n to p and collected at drain. The probability current density for the transmitted electron is $J_{qt}(E, \theta_i) = |t|^2 \langle \psi_t | \hat{J}^x | \psi_t \rangle$. Using the expressions for the transmitted wavefunction and charge

current density operator (Eq. 3) in this equation, we obtain the general expression for the charge current density

$$J_q(E, \theta_i) \equiv J_{qt} = \frac{s_t q v_F}{A} |t|^2 \cos \theta_{tr} e^{-\theta_{tI}} e^{-\kappa_{tx} L}, \quad (6)$$

where θ_{tr} and θ_{tI} are the real and imaginary parts of the transmission angle θ_t . Similarly, the probability current density for the incident wave is $J_{qi}(E, \theta_i) = s_i q v_F \cos \theta_i / A$ and the transmission probability is

$$T(E, \theta_i) \equiv J_{qt} / J_{qi} = \frac{\cos \theta_{tr}}{\cos \theta_i} |t|^2 e^{-\theta_{tI}} e^{-\kappa_{tx} L}. \quad (7)$$

Eq. 7 is the general form of transmission probability for electrons in graphene pn junction as presented in Refs. [9, 10] and valid for all energies in nn , pn and pp regime. Similarly, the spin current density at drain is

$$J_{syD}(E, \theta_i) = -\frac{\hbar v_F}{2 A} |t|^2 e^{-2\theta_{tI}} e^{-\kappa_{tx} L}. \quad (8)$$

The negative sign indicates that the spin current is carried by the down spin. The spin current at the source contact has two components: (1) the incident current $J_{syi}(E, \theta_i) = -\frac{\hbar v_F}{2A}$ and the reflected current $J_{syr}(E, \theta_i) = -\frac{\hbar v_F}{2A} |r|^2$. The total spin current density is then,

$$J_{syS}(E, \theta_i) = -\frac{\hbar v_F}{2 A} (1 + |r|^2) \quad (9)$$

where $|r|^2 = 1 - T(E, \theta_i)$. We note that unlike the incident and reflected components of charge currents, J_{syi} and J_{syr} have the same sign. This can be understood by noticing that when an electron with up-spin is reflected back from the pn junction interface, its spin is flipped due to the spin-momentum locking. Now, a down spin going to the left has the same spin current as an up spin going to the right. Hence, the spin currents due to the injected and the reflected electron add up enhancing the source spin current.

The total current is the sum of contributions from all electrons with positive group velocity along \hat{x} , weighted by the Fermi functions and integrated over all energies,

$$I = \frac{W}{2\pi} \int_{-\infty}^{\infty} dE D(E) [f_S(E) - f_D(E)] \times \int_{-\pi/2}^{\pi/2} d\theta A J(E, \theta) \quad (10)$$

where, $D(E) = \frac{1}{2\pi} \frac{|E + qV_n|}{\hbar^2 v_F^2}$ is the density of states which has the units of $\text{eV}^{-1} \text{m}^{-2}$, and $f_S(E)$ and $f_D(E)$ are the Fermi-Dirac distributions of source and drain, respectively. Eqs. 5-10 are valid for both symmetric and asymmetric built in potentials in nn , pn and pp regimes for all energies and hence can be used to calculate spin and charge current for large drain bias at room temperature.

For symmetric pn junction, within the barrier ($-qV_n < E < qV_p$), the transmission coefficient is dominated by

the exponential term in Eq. 5 and reduced to $t \approx e^{-\pi \hbar v_F k_i^2 d \sin^2 \theta_i / 2V_o}$. Hence, t is nonzero for electrons with very small incident angle ($\theta_i \ll \theta_c$). For these electrons, $e^{-\theta_{tI}} \approx 1$, $e^{\kappa_{tx} L} \approx 1$ and $\cos \theta_i \approx \cos \theta_{tr}$. Therefore, the transmission probability can be expressed as,

$$T(E, \theta_i) \approx e^{-\pi \hbar v_F k_i^2 d \sin^2 \theta_i / V_o} \quad (11)$$

which has the same form as the transmission probability in graphene pn junction [9, 10]. The charge current density in symmetric pn junction is then,

$$J_q(E, \theta_i) \approx q \frac{v_F}{A} [1 - R(E, \theta_i)] \quad (12)$$

and spin current densities at drain and source are

$$J_{syD,S}(E, \theta_i) \approx -\frac{\hbar v_F}{2 A} [1 \mp R(E, \theta_i)] \quad (13)$$

where $-$ and $+$ signs are for D and S respectively, and $R(E, \theta_i) = 1 - T(E, \theta_i)$ is the reflection probability. Now, the longitudinal spin Hall angle can be expressed as $\theta_H(E_F) = \int_{-\pi/2}^{\pi/2} d\theta J_{syS}(E_F, \theta) / \int_{-\pi/2}^{\pi/2} d\theta J_q(E_F, \theta)$ in the low bias limit. For symmetric pn junction, θ_H at the source contact reduces to the first expression in Eq. 1 where $R_{av} = \frac{1}{\pi} \int_{-\pi/2}^{\pi/2} d\theta e^{-\pi \hbar v_F k_i^2 d \sin^2 \theta_i / V_o}$ is the average reflection probability. When the Fermi energy is at the middle of the barrier, $\hbar v_F k_F = V_o/2$ and θ_H can be approximated as the last term of Eq. 1.

Eq. 11 clearly shows that $T(E, \theta_i)$ is nonzero only for electrons with very small incident angle. Hence, only these electrons are allowed to transmit through the TIPNJ. For all other modes, the reflection probability $R(E, \theta_i) \approx 1$ and those electrons are reflected back from the pn junction interface to the source. Thus, only few modes with small incident angle contribute to J_{syD} whereas all other modes contribute to J_{syS} as shown in the inset of Fig. 3. This picture is also consistent with the spin polarization of TIPNJ device. In the p side of the channel, only the transmitted waves exist and the spins of these electrons are aligned to $-y$ direction due to spin-momentum locking. Therefore, the p side of the channel is highly spin polarized as illustrated by blue in the inset of Fig. 2. On the other hand, in the n side of the channel, both the incident and the reflected waves exist with spins aligned to all the directions in $x - y$ plane. Therefore, the n region of the channel is unpolarized as indicated by green in the inset of Fig. 2. This is completely different from the uniform nn or pp device where the spin polarization is $2/\pi$ throughout the channel [20, 24]. Thus, the spin polarization shown in Fig. 2 is a key signature of spin filtering and amplification effect in TIPNJ, which can be experimentally measured by spin resolved scanning tunneling microscopy.

One way to measure θ_H is to pass the spin current through a ferromagnetic metal (FM) by using the FM as the source contact of TIPNJ. The spin current going through the FM will exert torque on the FM which

can be measured indirectly using spin torque ferromagnetic resonance technique[7] or directly by switching the magnetization (along $-\hat{y}$) of soft ferromagnets such as $(\text{Cr}_x\text{Bi}_y\text{Sb}_{1-x-y})_2\text{Te}_3$ at low temperature[8]. Once the magnetization of the FM is switched from $-\hat{y}$ to $+\hat{y}$, the current injection will stop (since spin up states cannot move towards right) and the system will reach the stable state. To switch the magnetization back to $-\hat{y}$ state, a complementary junction with another drain contact will be required. The switching of hard ferromagnets at room temperature may require further design considerations which is beyond the scope of this article.

In summary, we have shown that in TIPNJ, the chiral tunneling of helical states leads to real spin filtering effect while reducing the charge current. This is analogous to the pseudospin filtering in graphene pn junction. Due to spin-momentum locking in the surface of the TI, the reflected electrons give rise to enhancement of spin current at source which, in turn, leads to extremely large longitudinal spin Hall angle. Moreover, the longitudinal spin Hall angle and the spin currents at the source and drain are gate tunable and robust against edge reflection at room temperature. Any helical Dirac Fermionic system should exhibit gate tunable longitudinal spin Hall effect which may open a new way to design spintronic devices.

Acknowledgment. This work is supported by NRI IN-DEX center.

* masum.habib@virginia.edu

[1] B. A. Bernevig, T. L. Hughes, and S.-C. Zhang, *Science* **314**, 1757 (2006).

- [2] Y. Xia, D. Qian, D. Hsieh, L. Wray, A. Pal, H. Lin, A. Bansil, *et al.*, *Nature Physics* **5**, 398 (2009).
- [3] X.-L. Qi and S.-C. Zhang, *Reviews of Modern Physics* **83**, 1057 (2011).
- [4] L. Liu, C.-F. Pai, Y. Li, H. W. Tseng, D. C. Ralph, and R. A. Buhrman, *Science* **336**, 555 (2012).
- [5] O. Mosendz *et al.*, *Phys. Rev. Lett.* **104**, 046601 (2010).
- [6] L. Liu, T. Moriyama, D. C. Ralph, and R. A. Buhrman, *Phys. Rev. Lett.* **106**, 036601 (2011).
- [7] A. Mellnik *et al.*, *Nature* **511**, 449 (2014).
- [8] Y. Fan *et al.*, *Nature Materials* (2014).
- [9] V. V. Cheianov and V. I. Fal'ko, *Phys. Rev. B* **74**, 041403 (2006).
- [10] R. N. Sajjad, S. Sutar, J. Lee, and A. W. Ghosh, *Physical Review B* **86**, 155412 (2012).
- [11] R. N. Sajjad and A. W. Ghosh, *ACS nano* **7**, 9808 (2013).
- [12] A. F. Young and P. Kim, *Nat Phys* **5**, 222 (2009).
- [13] Z. Wu, F. Peeters, and K. Chang, *Applied Physics Letters* **98**, 162101 (2011).
- [14] R. Takahashi and S. Murakami, *Physical review letters* **107**, 166805 (2011).
- [15] J. Wang, X. Chen, B.-F. Zhu, and S.-C. Zhang, *Physical Review B* **85**, 235131 (2012).
- [16] J.-H. Gao, J. Yuan, W.-Q. Chen, Y. Zhou, and F.-C. Zhang, *Phys. Rev. Lett.* **106**, 057205 (2011).
- [17] J. Lee, J.-H. Lee, J. Park, J. S. Kim, and H.-J. Lee, *Physical Review X* **4** (2014).
- [18] J. Chen *et al.*, *Phys. Rev. Lett.* **105**, 176602 (2010).
- [19] L. Susskind, *Phys. Rev. D* **16**, 3031 (1977).
- [20] S. Hong, V. Diep, S. Datta, and Y. P. Chen, *Phys. Rev. B* **86**, 085131 (2012).
- [21] A. N. M. Zainuddin, S. Hong, L. Siddiqui, S. Srinivasan, and S. Datta, *Phys. Rev. B* **84**, 165306 (2011).
- [22] Y. Tserkovnyak and D. Loss, *Phys. Rev. Lett.* **108**, 187201 (2012).
- [23] Q.-f. Sun and X. Xie, *Phys. Rev. B* **72** (2005).
- [24] O. V. Yazyev, J. E. Moore, and S. G. Louie, *Physical review letters* **105**, 266806 (2010).